Volume 4
Number 1
January 2024
Pages 1–106

Environmental Science
Atmospheres

rsc.li/esatmospheres

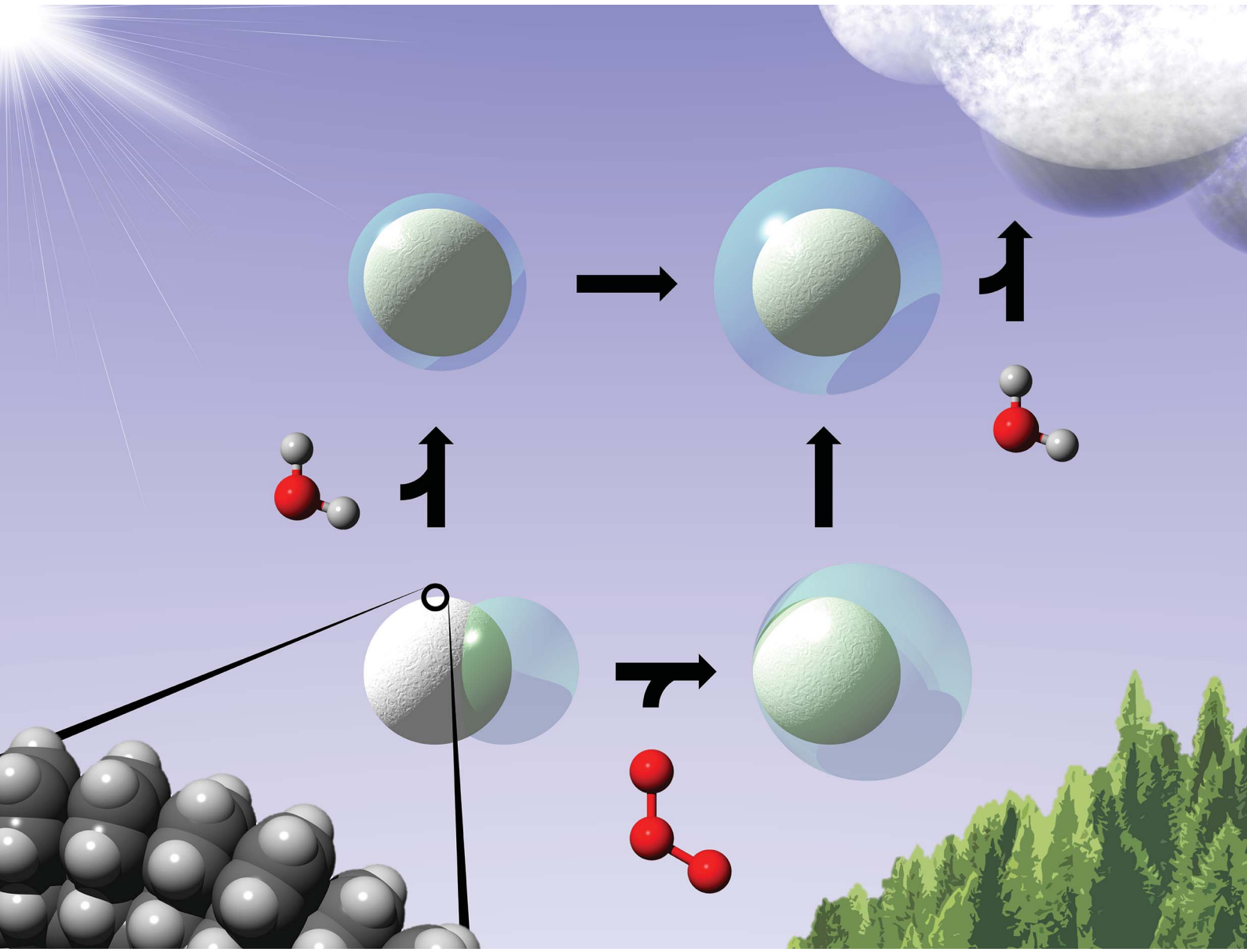

ISSN 2634-3606

ROYAL SOCIETY OF CHEMISTRY

COMMUNICATION
Elijah G. Schnitzler *et al.*
Partitioning of secondary organic aerosol onto nanoplastics leading to hygroscopic partially-engulfed particles

Environmental Science: Atmospheres

ROYAL SOCIETY OF CHEMISTRY

COMMUNICATION

View Article Online
View Journal | View Issue

Cite this: *Environ. Sci.: Atmos.*, 2024, **4**, 9

Received 1st July 2023
Accepted 13th November 2023

DOI: 10.1039/d3ea00103b

rsc.li/esatmospheres

Partitioning of secondary organic aerosol onto nanoplastics leading to hygroscopic partially-engulfed particles†

Katrina L. Raincrow, Habeeb H. Al-Mashala and Elijah G. Schnitzler *

Nanoplastics have been shown to be emitted into the atmosphere over land and the ocean and transported long distances to remote regions. During their atmospheric lifetime, nanoplastics may influence climate directly by absorbing and scattering sunlight and indirectly by enhancing ice or liquid cloud formation. Bare nanoplastics will not influence liquid cloud formation, since they are hydrophobic, but nanoplastics internally mixed with hygroscopic species during atmospheric aging have the potential to act as cloud condensation nuclei. Here, we report measurements of hygroscopic growth of initially 100, 200, and 250 nm polystyrene nanoplastics internally mixed with secondary organic aerosol (SOA) from the ozonolysis of α-pinene in a smog chamber. SOA formation and water uptake were quantified using parallel differential mobility analyzers at <10 and 90% relative humidity (RH), respectively. Interestingly, early in each experiment, at low SOA volumes, the mobility diameters of the humidified particles became smaller than those of the dry particles, despite certain water uptake. This discrepancy indicates that the particles at low RH have a non-spherical, partially-engulfed morphology. When they are humidified, the SOA takes up water, becomes less viscous, and coalesces around the nanoplastic, so the coated particles adopt a spherical morphology. Eventually, the SOA volume is high enough that the dry particles are also spherical, and the apparent volume of water scales linearly with the volume of SOA, as expected. A fit to measurements during this stage gives a hygroscopicity parameter of 0.02. Together, these observations have important implications on both the direct and indirect climate effects of nanoplastics in the atmosphere.

Environmental significance

Plastic particles with dimensions in the nanometer range, or nanoplastics, are emitted over land and the ocean into the atmosphere, where they are exposed to condensable products of the gas-phase oxidation of volatile organic compounds. These products can partition onto the particles, transforming the initially hydrophobic nanoplastics into potential cloud condensation nuclei. Here, we report appreciable hygroscopic growth, a prerequisite for cloud droplet activation, of polystyrene nanoplastics coated with secondary organic aerosol from the ozonolysis of α-pinene. Furthermore, we provide compelling evidence that under certain conditions, coating through partitioning can lead to partially-engulfed, rather than core–shell, morphologies, which may impact the direct and indirect climate effects of nanoplastics.

1. Introduction

Plastic particles with dimensions in the range of nanometers have been observed in the atmosphere.[1–3] These nanoplastics may be emitted into the environment directly or form from larger plastic pollution through chemical and physical processes.[4–6] They are small enough to be entrained over terrestrial sources, so their emission may increase with wind speed.[7,8] They can also be emitted over oceans,[9–11] where they tend to be concentrated at the sea surface microlayer, due to their low densities, ideally situated to be incorporated into sea spray aerosol upon wave breaking.[12–14] Because of their small dimensions, they can reside in the atmosphere for weeks, sometimes transported to remote regions, including the Arctic.[15,16] In turn, through wet and dry deposition, the nanoplastics are transferred from the atmospheric to the aquatic and terrestrial environments,[7,17,18] where they can continue to have a wide range of harmful influences on organisms.[19–21]

While they are in the atmosphere, nanoplastics may have direct and indirect effects on climate, by absorbing and scattering solar and terrestrial radiation and by influencing cloud formation, respectively.[22,23] Though all nanoplastics will scatter visible radiation, only those that are colored will strongly absorb at visible wavelengths. It is conceivable that colored nanoplastics whiten during their atmospheric lifetime, due to light-driven processing. Atmospheric aging is likely to also influence the indirect effects of nanoplastics, as the bare hydrophobic particles accumulate hygroscopic components. Bare and

Department of Chemistry, Oklahoma State University, Stillwater, OK 74078, USA. E-mail: elijah.schnitzler@okstate.edu

† Electronic supplementary information (ESI) available. See DOI: https://doi.org/10.1039/d3ea00103b

capped nanoplastics have been shown to act as ice nuclei.[24] Nanoplastics internally mixed with ammonium sulfate have been shown to take up water below saturation, so they have the potential to act as cloud condensation nuclei.[25] With aging, the nanoplastics are exposed to the condensable products of the gas-phase oxidation of volatile organic compounds, so they can also become internally mixed with secondary organic aerosol (SOA), much like black carbon, another solid carbonaceous aerosol.[26,27] The morphology of the hygroscopic SOA coatings on the nanoplastics will have implications on their direct and indirect climate effects.

Here, we report a series of smog chamber experiments designed to characterize the hygroscopicity and morphology of SOA-coated nanoplastics. The nanoplastic particles that were used in the chamber experiments are composed of the homopolymer polystyrene, with a proprietary surfactant to reduce aggregation in the concentrated aqueous suspensions during storage. Polystyrene has been observed in the form of microplastics in both the aquatic and terrestrial environments,[28,29] and it has been shown to be transported through the atmosphere to remote regions.[7,9] Polystyrene has also been used as a model microplastic species in many toxicological studies, shown to have diverse detrimental effects on marine and terrestrial organisms.[19–21,30,31] In aerosol science, spherical polystyrene particles are often used as standards for particle characterization, including size, hygroscopicity, and viscosity.[32–34] Three different sizes of polystyrene nanoplastics, first conditioned to ensure they were spherical with a uniform surface, were coated with SOA from the ozonolysis of α-pinene in a smog chamber at <10% relative humidity (RH). SOA formation and water uptake were measured using parallel differential mobility analyzers (DMAs), controlled at <10% and 90% RH, respectively, and coupled to a condensational particle counter (CPC). The changes in mobility diameter with aging and humidification contrast with the trends that would be expected for spherical core–shell particles, allowing us to identify partially-engulfed morphologies for SOA-coated nanoplastics under certain conditions.

2. Materials and methods

2.1. Introduction of nanoplastics

The nanoplastics were coated with SOA in a 1.2 m^3 smog chamber, illustrated in Fig. S1.† The chamber is constructed of perfluoroalkoxy (PFA) film (Ingeniven) and supported in a movable stainless-steel frame. Before each experiment, the chamber was flushed for at least 36 h with clean, dry air from a commercial zero-air generator (Aadco, 747-30). The background particle number concentration, measured with a CPC (TSI, 3750), was never greater than 5 cm^{-3} after flushing. The RH in the chamber was always less than 10%. Additional details are provided in the ESI.†

Aqueous suspensions of nanoplastics composed of polystyrene were prepared from commercial particle size standards (Polysciences, 64 000 Series), with nominal diameters of 100, 200, and 250 nm, by dilution with ultrapure water (18.2 MΩ cm) from a commercial water purification system (Thermo, Smart2Pure 3 UV). A given suspension was then sonicated while supplying a constant output atomizer (TSI, 3076). From the atomizer, the aerosolized nanoplastics were directed through two diffusion dryers, packed with indicating silica gel desiccant (Parker, DRP-14-10B), at a flow rate of 1.7 L min^{-1}. The dry nanoplastics were then directed to a custom-built thermal denuder, consisting of a 1.8 m length of 1/4″ copper tubing. In the first half of the copper tubing, the sample was heated to 473 K while, in the second half, it was cooled passively to 298 K. Heating in the thermal denuder did not produce additional particles, which have been observed for macroplastics heated in a tube furnace.[35] The conditioned nanoplastics were then injected into the smog chamber to a number concentration of at least 2000 cm^{-3}.

2.2. Introduction of α-pinene and ozone

After the nanoplastics were injected into the smog chamber, α-pinene was introduced as the SOA precursor using a syringe pump (Harvard Apparatus, 11 Plus), based on similar procedures reported in earlier studies.[36,37] The syringe contained a solution of (1*R*)-(+)-α-pinene (Acros, ≥98%, 80% ee) in hexane (Fisher, ≥98.5%), which it passed into a three-neck round-bottom flask. The flask was placed in a heating mantle, set to 340 K and filled with sand to distribute the heat evenly. The solution evaporated in the flask, and the vapor was carried into the smog chamber with clean, dry air, at a flow rate of 2 L min^{-1}. The initial mixing ratio of α-pinene in the chamber was 100 ppb. The nanoplastics and volatile organic compounds were allowed to mix in the chamber for 30 min.

After this mixing time, ozone was introduced into the chamber to begin the ozonolysis of α-pinene. Ozone was generated by irradiating air in a quartz tube with the emission of a Hg lamp (UVP, SOG-2) at a flow rate of 0.5 L min^{-1}. Ozone was introduced for the duration of each experiment, and its mixing ratio, measured with an ozone monitor (2B Technologies, 106 M), was never greater than 20 ppb.

2.3. Characterization of particles

The formation of SOA and the uptake of water were monitored during reaction in the chamber using parallel DMAs coupled to the CPC (see Fig. S1†). Particles sampled from the chamber were first passed through a wire-mesh denuder packed with catalyst (Carus, Carulite 200) for the destruction of ozone. Downstream of the catalyst, particles were sampled alternately through one of two branches of conditioning and classification.

In the first branch, the particles were size-selected at low RH using an electrostatic classifier (TSI, 3082), equipped with a soft X-ray advanced aerosol neutralizer (TSI, 3088) and a long DMA (TSI, 3081). The sample and sheath flow rates were 0.3 and 3 L min^{-1}, respectively. The RH of the recirculated sheath flow was controlled using a diffusion dryer to be <10% RH, to match that of the chamber. The sample and sheath RH values were monitored using calibrated sensors (Sensirion, SHT75).[38] The voltage of the DMA was set in LabVIEW, and the transmitted particles were directed to the CPC. The total flow rate of the CPC

was 1 L min^{-1}, so 0.7 L min^{-1} was drawn from the laboratory through a filter.

In the second branch, the particles were conditioned at high RH, specifically 90 ± 2%, using a Nafion membrane humidifier (Perma Pure, MD-110-48S-4) before being classified. After they passed through the humidifier, the particles were directed through a length of copper tubing to allow 30 s for equilibration at high RH. The particles were then directed to the second DMA, which was equipped the same as the first, with the same flow rates. The sheath flow of this DMA was set to 90 ± 2% RH, to match the humidified sample flow, using a second membrane humidifier. For each particle size spectrum (see Fig. S2†), or measurement distribution function,[39,40] the sample and sheath RH values agreed to within 2% during collection. The CPC sampled from the two DMAs alternately.

3. Results and discussion

Since our focus is on bare and SOA-coated nanoplastics, it was important that the initial particles were spherical with a uniform surface. In a previous study, a similar surfactant in aqueous suspensions of polystyrene was shown to form much smaller, hygroscopic particles, less than 100 nm in mobility diameter, externally mixed with the nanoplastics.[34] A comparison of the manufacturer-reported diameters, measured in suspension, and our mobility diameters, measured after aerosolization, are consistent with an external mixture (see Table S1†). To ensure the surface of the nanoplastics was uniform, we heated the particles to 473 K in the thermal denuder before injection into the smog chamber. If trace amounts of surfactant were present, this elevated temperature would promote desorption from the particle surface. Furthermore, this temperature is well above the glass transition temperature of polystyrene, 380 K, but below the melting point, 513 K.[41] Bispheres of polystyrene with point contacts have been shown to undergo coalescence to form spheres when heated above the glass transition temperature, due to surface tension, as the material becomes less viscous.[33] If any surface features were present, the decreased viscosity of the particles when heated would be expected to result in perfectly spherical particles upon cooling and vitrification. Volatility differential mobility analysis was performed by varying the temperature of the thermal denuder, and while no significant changes in mobility diameter were observed (see Fig. S3†), a slight drop is discernable for initially 100 nm particles just above the glass transition temperature (see Fig. S4†). Also, no water uptake to the conditioned polystyrene was observed, indicating that no traces of hygroscopic surfactant were present. Together, these observations confirm that the conditioned nanoplastics were spherical with a uniform surface.

The coatings of SOA were formed by gas-phase oxidation of α-pinene in the smog chamber. A representative experiment with initially 250 nm nanoplastics is shown in Fig. 1. SOA formation as a function of time is quantified here in terms of the diameter growth factor, Gfd, which is the ratio of the mobility diameter during reaction to that of the bare nanoplastics (see ESI†). At reaction time zero, the particles in the chamber were bare polystyrene, and the Gfd is one. As reaction progresses, oxidation products began partitioning to the particle phase, so the Gfd increases. Since the DMA was operated at <10% RH, like the chamber, water does not contribute to this growth. Since α-pinene was introduced with an excess of hexane, which is an effective hydroxyl radical scavenger without significantly altering the distribution of SOA species or the production of HO_2 radicals,[42–44] the SOA was strictly from the ozonolysis of α-pinene. By the end of the experiment, after nearly 250 min, the Gfd of the dry particles is 1.34 (see Fig. 1). Assuming the SOA coating is uniformly distributed, the average coating thickness is about 40 nm across the surface of the initially 250 nm nanoplastics. Comparable coating thicknesses have been measured for solid carbonaceous particles, specifically black carbon, exposed to ambient air in Houston, USA, for 10 to 15 h.[45] The apparent volume growth factor, Gfv, can be calculated from this timeseries, assuming the particles are spherical for the entirety of the experiment (see ESI†). Since the reaction kinetics can vary slightly between experiments, this apparent Gfv, instead of reaction time, is used as an independent variable in the subsequent discussion. In turn, the mass growth factor, Gfm, can be calculated to reach 2.68 at the end of the experiment (see Fig. S5†). The densities of polystyrene, α-pinene SOA, and water are taken as 1.05, 1.28, and 1.00 g cm^{-3}, respectively.[46,47] By the end of the experiment, the dry particles are 63% SOA by mass (see Fig. S6†). Importantly, given the second-order rate constant for the ozonolysis of α-pinene, 8.4 × 10^{-17} cm^3 mol^{-1} s^{-1},[48] and the upper limit for the mixing ratio of ozone, 20 ppb, 55% of the initial α-pinene was still present at the end of the experiment. By design, these reaction conditions allowed slow, steady growth of the coatings and ensured their composition was relatively uniform, as first-generation products formed for the duration of the experiment.

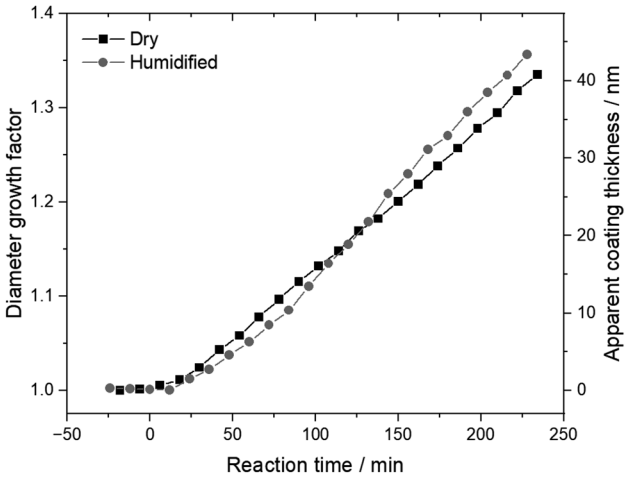

Fig. 1 Diameter growth factor and apparent coating thickness as functions of reaction time in the smog chamber for a representative experiment with initially 250 nm nanoplastics.

Additional growth of the SOA-coated nanoplastics due to water uptake was measured by conditioning and classifying the particles at high RH. In κ-Köhler theory, water uptake is

governed by the hygroscopicity parameter κ,[49,50] which is defined by its impact on water activity, a_w, according to eqn (1).

$$\frac{1}{a_w} = 1 + \kappa \frac{V_s}{V_w} \quad (1)$$

Here, V_s is the volume of the dry, water-soluble particle before uptake, and V_w is the volume of water after uptake. In the smog chamber experiments, only the SOA coating is water-soluble, so V_s is taken as the volume of SOA, V_{SOA}. Eqn (1) can be rearranged to relate the volume of water to V_{SOA} according to eqn (2).

$$V_w = \kappa \frac{a_w}{(1 - a_w)} V_{SOA} \quad (2)$$

Typically, individual κ values are reported for SOA from distinct precursors, although κ may increase slightly with further oxidative aging of the SOA, in terms of the oxygen-to-carbon ratio.[51] In hygroscopic tandem DMA experiments, V_{SOA} is held constant, by setting the voltage of the first DMA, and the activity of water is ramped up to increase the volume of water, V_w.[52–54] Here, in contrast, the volume of SOA is increased, and the activity of water is held constant. We assume that the activity of water is equal the saturation ratio, neglecting the Kelvin effect for the SOA-coated particles.[49,50] Since κ and a_w are steady, the volume of water taken up by the particles will increase linearly with the volume of SOA partitioned onto the polystyrene. Surprisingly, between 0 and about 100 min, the Gfd of the humidified particles is lower than that of the dry particles (see Fig. 1). At 125 min, the two timeseries intersect, and afterwards the humidified particles are larger than the dry particles, as expected. Towards the end of the experiment, the two timeseries increase proportionally. In one experiment, the parallel DMAs were interchanged to rule out instrumental artefacts, yielding the same trends.

What is the origin of these unexpected observations? The difference between the Gfd values for the dry and humidified particles is quantified in terms of the hygroscopic volume growth factor, HGfv.[26,55] When the ozonolysis in the chamber begins, the HGfv decreases, eventually to a minimum value of about 0.95, before beginning to increase (see Fig. S7†). It returns to unity when the timeseries of Gfd intersect, *e.g.*, at 125 min in Fig. 1. With further reaction, the HGfv increases rapidly to reach a plateau at about 1.07 after 150 min. If this trend in HGfv is plotted as a function of the apparent SOA coating volume, as shown in Fig. 2, the plateau occurs at a Gfv of about 2. Analogous trends for initially 100 and 200 nm nanoplastics are shown in Fig. S8.† The apparent volume of water can also be calculated from this timeseries. Note that the apparent volumes of SOA and water are based on the assumption that the particles are spherical throughout each experiment. Since the nanoplastics are spherical to begin the experiment, as described above, this assumption would be true if the coating occurred uniformly across the nanoplastic surface. The seeming loss of water from already dry particles that are non-volatile demonstrates that the coated particles adopt partially-engulfed, rather than core–shell, morphology at small SOA volumes. SOA from α-pinene is known to be glassy at low RH but less viscous at high RH.[56] Consequently, the coated nanoplastics classified by the DMA at

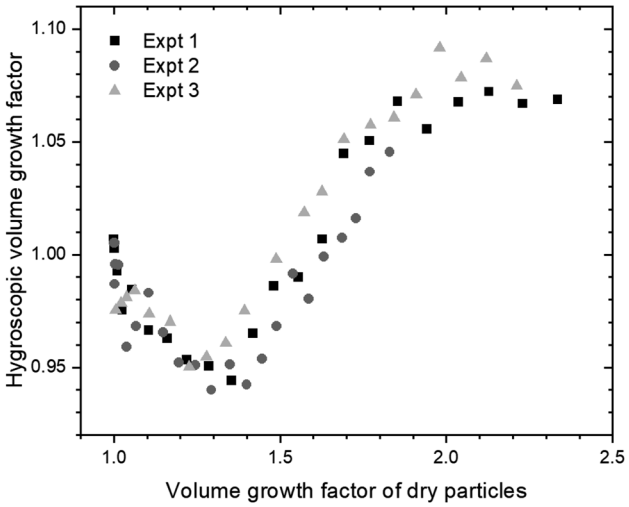

Fig. 2 Hygroscopic volume growth factor as a function of the volume growth factor of the dry particles, a measure of the SOA coating volume, for three experiments with initially 250 nm nanoplastics, illustrating intra- and inter-experiment variability. There is more scatter in the hygroscopic volume growth factor than in the individual time series of diameter growth factors, because the hygroscopic volume growth factor is a measure of the small difference between these time series.

low RH retained the non-spherical morphology of particles in the dry chamber, whereas those classified by the DMA at high RH coalesced to give spherical morphology. Importantly, although smaller values have been determined in the free molecular regime,[57] the dynamic shape factor, χ, of bispheres in the continuum (or viscous) flow regime is known to be 1.10,[58,59] which is more than enough to allow for the degree of restructuring observed here and broadly consistent with partially-engulfed morphology at low RH.

The relationship between the volume of water and the volume of SOA, according to eqn (2), can further highlight these differences in morphology. Since κ and a_w are steady, the relationship should be linear. As shown in Fig. 3, the apparent volume of water drops below zero at early reaction times, *i.e.*, small SOA volumes. During this period, the particles in the chamber, at low RH, have partially-engulfed morphology. When they are humidified before classification in the second DMA, the SOA takes up water, transitions to liquid, and fully encapsulates the polystyrene to give spherical core–shell particles at all SOA coating volumes. At low RH, significantly more SOA volume must accumulate to fully encapsulate the polystyrene and give spherical particles; in this case, the polystyrene may be uncentered in the SOA coating. The apparent volume of water increases and returns to zero at the intersection of the Gfd timeseries for the dry and humified particles. Once the particles become spherical at low RH, at large SOA volumes, the volume of water scales linearly with the SOA volume, as initially expected. The SOA volume required to reach spherical morphology at low RH increases with the diameter of the nanoplastics (see Fig. 3), because they must be fully encapsulated.

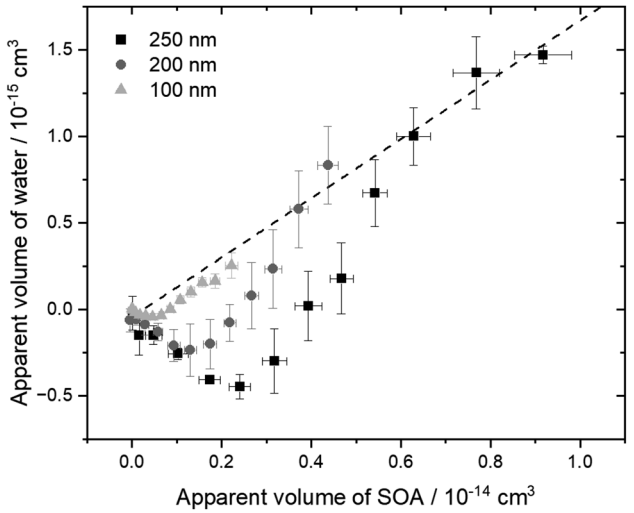

Fig. 3 Apparent volume of water as a function of the apparent volume of SOA, as if the particles were spherical for the duration of each experiment. Measurements from three experiments for each initial diameter were concatenated, sorted from smallest SOA volume to largest, and averaged to give the error bars, which indicate one standard deviation for five adjacent datapoints. The individual experiments are shown in Fig. S9.†

A fit of eqn (2) to the data for spherical particles at sufficient SOA volumes can provide a measure of the hygroscopicity of the α-pinene SOA. Since the activity, or saturation ratio, of water is constant throughout the coating experiments, the slope of the line in Fig. 3 can be divided by the term $a_w/(1 - a_w)$ to give a value of 0.02 for the hygroscopicity parameter κ. This value is at the lower end of the range previously measured for pure α-pinene SOA, which extends from about 0.02 to 0.06.[51] Our choice of a biogenic volatile organic compound as the SOA precursor that has a lower κ value than most anthropogenic precursors was strategic,[51] allowing us to focus on the lower range of Gfd values, where the evidence for partially-engulfed particles occurs. For instance, greater hygroscopic growth over the same reaction time likely would have obscured the coalescence observed here. Furthermore, our choice of mixing ratios, leading to first-generation ozonolysis products for the duration of each experiment, allowed us to rule out evaporation, *e.g.*, due to hydrolysis,[60] because the fraction evaporated would be consistent throughout the experiments, rather than evolving as shown in Fig. 2. To the best of our knowledge, these are the first smog chamber observations to demonstrate that SOA coating of any solid carbonaceous particles can lead to partially-engulfed particles. Nanoplastics composed of other polymers, including polyethylene and polypropylene, which are also abundant in plastic litter,[61] should be investigated in the future.

4. Atmospheric implications

These observations have significant implications on the fate and impact of nanoplastics in the atmosphere. Nanoplastics have been shown to be emitted directly over land or resuspended over the ocean.[7,10] When emitted from the ocean, the nanoplastics are likely internally mixed with some mass fraction of sea spray aerosol components.[12,13,62] When emitted over land, the nanoplastics may be bare. The bare nanoplastics are hydrophobic, so they will not take up water below saturation nor influence liquid cloud formation[23,63] except through heterogeneous nucleation, similar to black carbon.[26,55,64] On the other hand, the bare nanoplastics may influence ice cloud formation by providing a solid surface for crystallization.[23,24] The bare nanoplastics will be exposed to oxidants, which may introduce polar, hydrophilic functional groups at the surface.[65] The bare nanoplastics will also be exposed to the oxidation products of volatile organic compounds in the atmosphere.[48,66] These products will partition according to their saturation vapor pressures,[67,68] resulting in some volume of SOA internally mixed with the nanoplastics. Nanoplastics internally mixed with other species have been observed in ambient samples.[18] Here, we show that nanoplastics internally mixed with α-pinene SOA can undergo hygroscopic growth and, in turn, will enhance liquid cloud formation, according to the polarities of the SOA constituents.[50,51] We also show for the first time that SOA coating can lead to partially-engulfed particles when the SOA is a solid. The RH conditions required for the SOA to be sufficiently viscous will vary with the precursor,[56,69,70] so intermediate RH values most representative of atmospheric conditions should be explored in future work. Furthermore, if aggregates of nanoplastics are emitted into the atmosphere or form through coagulation, SOA coatings may lead to restructuring at elevated RH, when the SOA is a liquid,[55] similar to what has been observed for aggregates of black carbon.[71,72] The morphology of the SOA-coated particles resulting from these coupled processes will play a vital role in both the direct and indirect effects of nanoplastics on climate.[22,23]

Conflicts of interest

There are no conflicts to declare.

Acknowledgements

The authors thank Ed Wright for technical support and Gary Osborn for electrical support. They also thank Frank Blum (Oklahoma State University) and Jorge Gonzalez-Estrella (Oklahoma State University) for helpful discussions on the properties and processing of nanoplastics in the environment and two anonymous reviewers for their helpful comments. This research was funded by Oklahoma State University and the Oklahoma Center for the Advancement of Science and Technology (OCAST), through grant PS21-004.

References

1 M. González-Pleiter, C. Edo, Á. Aguilera, D. Viúdez-Moreiras, G. Pulido-Reyes, E. González-Toril, S. Osuna, G. de Diego-Castilla, F. Leganés, F. Fernández-Piñas and R. Rosal, Occurrence and Transport of Microplastics Sampled within and above the Planetary Boundary Layer, *Sci. Total*

Environ., 2021, **761**, 143213, DOI: 10.1016/j.scitotenv.2020.143213.

2 J. M. Levermore, T. E. L. Smith, F. J. Kelly and S. L. Wright, Detection of Microplastics in Ambient Particulate Matter Using Raman Spectral Imaging and Chemometric Analysis, *Anal. Chem.*, 2020, **92**(13), 8732–8740, DOI: 10.1021/acs.analchem.9b05445.

3 Y. Li, L. Shao, W. Wang, M. Zhang, X. Feng, W. Li and D. Zhang, Airborne Fiber Particles: Types, Size and Concentration Observed in Beijing, *Sci. Total Environ.*, 2020, **705**, 135967, DOI: 10.1016/j.scitotenv.2019.135967.

4 Z. Liu, Y. Zhu, S. Lv, Y. Shi, S. Dong, D. Yan, X. Zhu, R. Peng, A. A. Keller and Y. Huang, Quantifying the Dynamics of Polystyrene Microplastics UV-Aging Process, *Environ. Sci. Technol. Lett.*, 2022, **9**(1), 50–56, DOI: 10.1021/acs.estlett.1c00888.

5 A. Bianco, F. Sordello, M. Ehn, D. Vione and M. Passananti, Degradation of Nanoplastics in the Environment: Reactivity and Impact on Atmospheric and Surface Waters, *Sci. Total Environ.*, 2020, **742**, 140413, DOI: 10.1016/j.scitotenv.2020.140413.

6 Z. Wang, A. Pilechi, M. Fok Cheung and P. A. Ariya, In-Situ and Real-Time Nano/Microplastic Coatings and Dynamics in Water Using Nano-DIHM: A Novel Capability for the Plastic Life Cycle Research, *Water Res.*, 2023, **235**, 119898, DOI: 10.1016/j.watres.2023.119898.

7 J. Brahney, M. Hallerud, E. Heim, M. Hahnenberger and S. Sukumaran, Plastic Rain in Protected Areas of the United States, *Science*, 2020, **368**(6496), 1257–1260, DOI: 10.1126/science.aaz5819.

8 A. I. S. Purwiyanto, T. Prartono, E. Riani, Y. Naulita, M. R. Cordova and A. F. Koropitan, The Deposition of Atmospheric Microplastics in Jakarta-Indonesia: The Coastal Urban Area, *Mar. Pollut. Bull.*, 2022, **174**, 113195, DOI: 10.1016/j.marpolbul.2021.113195.

9 S. Allen, D. Allen, V. R. Phoenix, G. Le Roux, P. Durántez Jiménez, A. Simonneau, S. Binet and D. Galop, Atmospheric Transport and Deposition of Microplastics in a Remote Mountain Catchment, *Nat. Geosci.*, 2019, **12**(5), 339–344, DOI: 10.1038/s41561-019-0335-5.

10 S. Allen, D. Allen, K. Moss, G. L. Roux, V. R. Phoenix and J. E. Sonke, Examination of the Ocean as a Source for Atmospheric Microplastics, *PLoS One*, 2020, **15**(5), e0232746, DOI: 10.1371/journal.pone.0232746.

11 D. Allen, S. Allen, S. Abbasi, A. Baker, M. Bergmann, J. Brahney, T. Butler, R. A. Duce, S. Eckhardt, N. Evangeliou, T. Jickells, M. Kanakidou, P. Kershaw, P. Laj, J. Levermore, D. Li, P. Liss, K. Liu, N. Mahowald, P. Masque, D. Materić, A. G. Mayes, P. McGinnity, I. Osvath, K. A. Prather, J. M. Prospero, L. E. Revell, S. G. Sander, W. J. Shim, J. Slade, A. Stein, O. Tarasova and S. Wright, Microplastics and Nanoplastics in the Marine-Atmosphere Environment, *Nat. Rev. Earth Environ.*, 2022, **3**(6), 393–405, DOI: 10.1038/s43017-022-00292-x.

12 J. M. Schiffer, L. E. Mael, K. A. Prather, R. E. Amaro and V. H. Grassian, Sea Spray Aerosol: Where Marine Biology Meets Atmospheric Chemistry, *ACS Cent. Sci.*, 2018, **4**(12), 1617–1623, DOI: 10.1021/acscentsci.8b00674.

13 S. Liu, C.-C. Liu, K. D. Froyd, G. P. Schill, D. M. Murphy, T. P. Bui, J. M. Dean-Day, B. Weinzierl, M. Dollner, G. S. Diskin, G. Chen and R.-S. Gao, Sea Spray Aerosol Concentration Modulated by Sea Surface Temperature, *Proc. Natl. Acad. Sci. U.S.A.*, 2021, **118**(9), e2020583118, DOI: 10.1073/pnas.2020583118.

14 A. I. Catarino, M. C. León, Y. Li, S. Lambert, M. Vercauteren, J. Asselman, C. R. Janssen, G. Everaert and M. De Rijcke, Micro- and Nanoplastics Transfer from Seawater to the Atmosphere through Aerosolization under Controlled Laboratory Conditions, *Mar. Pollut. Bull.*, 2023, **192**, 115015, DOI: 10.1016/j.marpolbul.2023.115015.

15 N. Evangeliou, H. Grythe, Z. Klimont, C. Heyes, S. Eckhardt, S. Lopez-Aparicio and A. Stohl, Atmospheric Transport Is a Major Pathway of Microplastics to Remote Regions, *Nat. Commun.*, 2020, **11**(1), 3381, DOI: 10.1038/s41467-020-17201-9.

16 M. Bergmann, F. Collard, J. Fabres, G. W. Gabrielsen, J. F. Provencher, C. M. Rochman, E. van Sebille and M. B. Tekman, Plastic Pollution in the Arctic, *Nat. Rev. Earth Environ.*, 2022, **3**(5), 323–337, DOI: 10.1038/s43017-022-00279-8.

17 S. Abbasi and A. Turner, Dry and Wet Deposition of Microplastics in a Semi-Arid Region (Shiraz, Iran), *Sci. Total Environ.*, 2021, **786**, 147358, DOI: 10.1016/j.scitotenv.2021.147358.

18 L. Cai, J. Wang, J. Peng, Z. Tan, Z. Zhan, X. Tan and Q. Chen, Characteristic of Microplastics in the Atmospheric Fallout from Dongguan City, China: Preliminary Research and First Evidence, *Environ. Sci. Pollut. Res.*, 2017, **24**(32), 24928–24935, DOI: 10.1007/s11356-017-0116-x.

19 Z. Sobhani, L. Panneerselvan, C. Fang, R. Naidu and M. Megharaj, Chronic and Transgenerational Effects of Polystyrene Microplastics at Environmentally Relevant Concentrations in Earthworms (Eisenia Fetida), *Environ. Toxicol. Chem.*, 2021, **40**(8), 2240–2246, DOI: 10.1002/etc.5072.

20 M. Cole, P. Lindeque, E. Fileman, C. Halsband and T. S. Galloway, The Impact of Polystyrene Microplastics on Feeding, Function and Fecundity in the Marine Copepod Calanus Helgolandicus, *Environ. Sci. Technol.*, 2015, **49**(2), 1130–1137, DOI: 10.1021/es504525u.

21 R. Sussarellu, M. Suquet, Y. Thomas, C. Lambert, C. Fabioux, M. E. J. Pernet, N. Le Goïc, V. Quillien, C. Mingant, Y. Epelboin, C. Corporeau, J. Guyomarch, J. Robbens, I. Paul-Pont, P. Soudant and A. Huvet, Oyster Reproduction Is Affected by Exposure to Polystyrene Microplastics, *Proc. Natl. Acad. Sci. U.S.A.*, 2016, **113**(9), 2430–2435, DOI: 10.1073/pnas.1519019113.

22 L. E. Revell, P. Kuma, E. C. Le Ru, W. R. C. Somerville and S. Gaw, Direct Radiative Effects of Airborne Microplastics, *Nature*, 2021, **598**(7881), 462–467, DOI: 10.1038/s41586-021-03864-x.

23 M. Aeschlimann, G. Li, Z. A. Kanji and D. M. Mitrano, Potential Impacts of Atmospheric Microplastics and

Nanoplastics on Cloud Formation Processes, *Nat. Geosci.*, 2022, **15**(12), 967–975, DOI: 10.1038/s41561-022-01051-9.

24 M. Ganguly and P. A. Ariya, Ice Nucleation of Model Nanoplastics and Microplastics: A Novel Synthetic Protocol and the Influence of Particle Capping at Diverse Atmospheric Environments, *ACS Earth Space Chem.*, 2019, **3**(9), 1729–1739, DOI: 10.1021/acsearthspacechem.9b00132.

25 A. Bain and T. C. Preston, Hygroscopicity of Microplastic and Mixed Microplastic Aqueous Ammonium Sulfate Systems, *Environ. Sci. Technol.*, 2021, **55**(17), 11775–11783, DOI: 10.1021/acs.est.1c04272.

26 C. Qiu, A. F. Khalizov and R. Zhang, Soot Aging from OH-Initiated Oxidation of Toluene, *Environ. Sci. Technol.*, 2012, **46**(17), 9464–9472, DOI: 10.1021/es301883y.

27 E. G. Schnitzler, A. Dutt, A. M. Charbonneau, J. S. Olfert and W. Jäger, Soot Aggregate Restructuring Due to Coatings of Secondary Organic Aerosol Derived from Aromatic Precursors, *Environ. Sci. Technol.*, 2014, **48**(24), 14309–14316, DOI: 10.1021/es503699b.

28 K. L. Ng and J. P. Obbard, Prevalence of Microplastics in Singapore's Coastal Marine Environment, *Mar. Pollut. Bull.*, 2006, **52**(7), 761–767, DOI: 10.1016/j.marpolbul.2005.11.017.

29 G. F. Schirinzi, M. Llorca, R. Seró, E. Moyano, D. Barceló, E. Abad and M. Farré, Trace Analysis of Polystyrene Microplastics in Natural Waters, *Chemosphere*, 2019, **236**, 124321, DOI: 10.1016/j.chemosphere.2019.07.052.

30 Y. Mao, H. Ai, Y. Chen, Z. Zhang, P. Zeng, L. Kang, W. Li, W. Gu, Q. He and H. Li, Phytoplankton Response to Polystyrene Microplastics: Perspective from an Entire Growth Period, *Chemosphere*, 2018, **208**, 59–68, DOI: 10.1016/j.chemosphere.2018.05.170.

31 Y. Wang, D. Zhang, M. Zhang, J. Mu, G. Ding, Z. Mao, Y. Cao, F. Jin, Y. Cong, L. Wang, W. Zhang and J. Wang, Effects of Ingested Polystyrene Microplastics on Brine Shrimp, Artemia Parthenogenetica, *Environ. Pollut.*, 2019, **244**, 715–722, DOI: 10.1016/j.envpol.2018.10.024.

32 J. Fernandez de la Mora, J. Kramar, N. Farkas, S. Papanu and R. Dana, Singularly Narrow Size Distributions of 200 nm Polystyrene Latex Spheres Determined by High Resolution Mobility Analysis, *J. Aerosol Sci.*, 2023, **170**, 106158, DOI: 10.1016/j.jaerosci.2023.106158.

33 A. J. Trevitt, P. J. Wearne and E. J. Bieske, Coalescence of Levitated Polystyrene Microspheres, *J. Aerosol Sci.*, 2009, **40**(5), 431–438, DOI: 10.1016/j.jaerosci.2009.01.001.

34 C.-N. Mao, K. Gohil and A. A. Asa-Awuku, A Single-Parameter Hygroscopicity Model for Functionalized Insoluble Aerosol Surfaces, *Atmos. Chem. Phys.*, 2022, **22**(19), 13219–13228, DOI: 10.5194/acp-22-13219-2022.

35 P. J. Wlasits, A. Stoellner, G. Lattner, K. Maggauer and P. M. Winkler, Size Characterization and Detection of Aerosolized Nanoplastics Originating from Evaporated Thermoplastics, *Aerosol Sci. Technol.*, 2022, **56**(2), 176–185, DOI: 10.1080/02786826.2021.1998339.

36 Y. Qin, J. Ye, P. Ohno, J. Zhai, Y. Han, P. Liu, J. Wang, R. A. Zaveri and S. T. Martin, Humidity Dependence of the Condensational Growth of α-Pinene Secondary Organic Aerosol Particles, *Environ. Sci. Technol.*, 2021, **55**(21), 14360–14369, DOI: 10.1021/acs.est.1c01738.

37 M. Shrestha, Y. Zhang, C. J. Ebben, S. T. Martin and F. M. Geiger, Vibrational Sum Frequency Generation Spectroscopy of Secondary Organic Material Produced by Condensational Growth from α-Pinene Ozonolysis, *J. Phys. Chem. A*, 2013, **117**(35), 8427–8436, DOI: 10.1021/jp405065d.

38 K. L. Betz, C. T. Calvert, H. H. Al-Mashala and E. G. Schnitzler, Hygroscopicity of Secondary Brown Carbon Aerosol from Aqueous Photo-Oxidation of Phenolic Precursors, *ACS Earth Space Chem.*, 2022, **6**(11), 2609–2618, DOI: 10.1021/acsearthspacechem.2c00132.

39 M. Gysel, G. B. McFiggans and H. Coe, Inversion of Tandem Differential Mobility Analyser (TDMA) Measurements, *J. Aerosol Sci.*, 2009, **40**(2), 134–151, DOI: 10.1016/j.jaerosci.2008.07.013.

40 M. R. Stolzenburg and P. H. McMurry, Equations Governing Single and Tandem DMA Configurations and a New Lognormal Approximation to the Transfer Function, *Aerosol Sci. Technol.*, 2008, **42**(6), 421–432, DOI: 10.1080/02786820802157823.

41 J. Rieger, The Glass Transition Temperature of Polystyrene, *J. Therm. Anal.*, 1996, **46**(3), 965–972, DOI: 10.1007/BF01983614.

42 M. D. Keywood, V. Varutbangkul, R. Bahreini, R. C. Flagan and J. H. Seinfeld, Secondary Organic Aerosol Formation from the Ozonolysis of Cycloalkenes and Related Compounds, *Environ. Sci. Technol.*, 2004, **38**(15), 4157–4164, DOI: 10.1021/es035363o.

43 K. Sato, S. Inomata, J.-H. Xing, T. Imamura, R. Uchida, S. Fukuda, K. Nakagawa, J. Hirokawa, M. Okumura and S. Tohno, Effect of OH Radical Scavengers on Secondary Organic Aerosol Formation from Reactions of Isoprene with Ozone, *Atmos. Environ.*, 2013, **79**, 147–154, DOI: 10.1016/j.atmosenv.2013.06.036.

44 A. L. Putman, J. H. Offenberg, R. Fisseha, S. Kundu, T. A. Rahn and L. R. Mazzoleni, Ultrahigh-Resolution FT-ICR Mass Spectrometry Characterization of α-Pinene Ozonolysis SOA, *Atmos. Environ.*, 2012, **46**, 164–172, DOI: 10.1016/j.atmosenv.2011.10.003.

45 J. Peng, M. Hu, S. Guo, Z. Du, J. Zheng, D. Shang, M. L. Zamora, L. Zeng, M. Shao, Y.-S. Wu, J. Zheng, Y. Wang, C. R. Glen, D. R. Collins, M. J. Molina and R. Zhang, Markedly Enhanced Absorption and Direct Radiative Forcing of Black Carbon under Polluted Urban Environments, *Proc. Natl. Acad. Sci. U.S.A.*, 2016, **113**(16), 4266–4271, DOI: 10.1073/pnas.1602310113.

46 S. Nakao, P. Tang, X. Tang, C. H. Clark, L. Qi, E. Seo, A. Asa-Awuku and D. Cocker, Density and Elemental Ratios of Secondary Organic Aerosol: Application of a Density Prediction Method, *Atmos. Environ.*, 2013, **68**, 273–277, DOI: 10.1016/j.atmosenv.2012.11.006.

47 H. Saathoff, K.-H. Naumann, O. Möhler, Å. M. Jonsson, M. Hallquist, A. Kiendler-Scharr, T. F. Mentel, R. Tillmann and U. Schurath, Temperature Dependence of Yields of Secondary Organic Aerosols from the Ozonolysis of α-

Pinene and Limonene, *Atmos. Chem. Phys.*, 2009, **9**(5), 1551–1577, DOI: 10.5194/acp-9-1551-2009.

48 R. Atkinson and J. Arey, Atmospheric Degradation of Volatile Organic Compounds, *Chem. Rev.*, 2003, **103**(12), 4605–4638, DOI: 10.1021/cr0206420.

49 S. M. Kreidenweis, M. D. Petters and P. J. DeMott, Single-Parameter Estimates of Aerosol Water Content, *Environ. Res. Lett.*, 2008, **3**(3), 035002, DOI: 10.1088/1748-9326/3/3/035002.

50 M. D. Petters and S. M. Kreidenweis, A Single Parameter Representation of Hygroscopic Growth and Cloud Condensation Nucleus Activity, *Atmos. Chem. Phys.*, 2007, **7**(8), 1961–1971, DOI: 10.5194/acp-7-1961-2007.

51 D. F. Zhao, A. Buchholz, B. Kortner, P. Schlag, F. Rubach, H. Fuchs, A. Kiendler-Scharr, R. Tillmann, A. Wahner, Å. K. Watne, M. Hallquist, J. M. Flores, Y. Rudich, K. Kristensen, A. M. K. Hansen, M. Glasius, I. Kourtchev, M. Kalberer and T. F. Mentel, Cloud Condensation Nuclei Activity, Droplet Growth Kinetics, and Hygroscopicity of Biogenic and Anthropogenic Secondary Organic Aerosol (SOA), *Atmos. Chem. Phys.*, 2016, **16**(2), 1105–1121, DOI: 10.5194/acp-16-1105-2016.

52 K. A. Malek, K. Gohil, H. A. Al-Abadleh and A. A. Asa-Awuku, Hygroscopicity of Polycatechol and Polyguaiacol Secondary Organic Aerosol in Sub- and Supersaturated Water Vapor Environments, *Environ. Sci.: Atmos.*, 2022, **2**(1), 24–33, DOI: 10.1039/D1EA00063B.

53 E. F. Mikhailov and S. S. Vlasenko, High-Humidity Tandem Differential Mobility Analyzer for Accurate Determination of Aerosol Hygroscopic Growth, Microstructure, and Activity Coefficients over a Wide Range of Relative Humidity, *Atmos. Meas. Tech.*, 2020, **13**(4), 2035–2056, DOI: 10.5194/amt-13-2035-2020.

54 X. Fan, J. Liu, F. Zhang, L. Chen, D. Collins, W. Xu, X. Jin, J. Ren, Y. Wang, H. Wu, S. Li, Y. Sun and Z. Li, Contrasting Size-Resolved Hygroscopicity of Fine Particles Derived by HTDMA and HR-ToF-AMS Measurements between Summer and Winter in Beijing: The Impacts of Aerosol Aging and Local Emissions, *Atmos. Chem. Phys.*, 2020, **20**(2), 915–929, DOI: 10.5194/acp-20-915-2020.

55 K. K. Leung, E. G. Schnitzler, W. Jäger and J. S. Olfert, Relative Humidity Dependence of Soot Aggregate Restructuring Induced by Secondary Organic Aerosol: Effects of Water on Coating Viscosity and Surface Tension, *Environ. Sci. Technol. Lett.*, 2017, **4**(9), 386–390, DOI: 10.1021/acs.estlett.7b00298.

56 L. Renbaum-Wolff, J. W. Grayson, A. P. Bateman, M. Kuwata, M. Sellier, B. J. Murray, J. E. Shilling, S. T. Martin and A. K. Bertram, Viscosity of α-Pinene Secondary Organic Material and Implications for Particle Growth and Reactivity, *Proc. Natl. Acad. Sci. U.S.A.*, 2013, **110**(20), 8014–8019, DOI: 10.1073/pnas.1219548110.

57 A. Zelenyuk, Y. Cai and D. Imre, From Agglomerates of Spheres to Irregularly Shaped Particles: Determination of Dynamic Shape Factors from Measurements of Mobility and Vacuum Aerodynamic Diameters, *Aerosol Sci. Technol.*, 2006, **40**(3), 197–217, DOI: 10.1080/02786820500529406.

58 B. E. Dahneke, Slip Correction Factors for Nonspherical Bodies—I Introduction and Continuum Flow, *J. Aerosol Sci.*, 1973, **4**(2), 139–145, DOI: 10.1016/0021-8502(73)90065-7.

59 B. Dahneke, Viscous Resistance of Straight-Chain Aggregates of Uniform Spheres, *Aerosol Sci. Technol.*, 1982, **1**(2), 179–185, DOI: 10.1080/02786828208958586.

60 A. Buchholz, A. T. Lambe, A. Ylisirniö, Z. Li, O.-P. Tikkanen, C. Faiola, E. Kari, L. Hao, O. Luoma, W. Huang, C. Mohr, D. R. Worsnop, S. A. Nizkorodov, T. Yli-Juuti, S. Schobesberger and A. Virtanen, Insights into the O:C-Dependent Mechanisms Controlling the Evaporation of α-Pinene Secondary Organic Aerosol Particles, *Atmos. Chem. Phys.*, 2019, **19**(6), 4061–4073, DOI: 10.5194/acp-19-4061-2019.

61 A. E. Schwarz, T. N. Ligthart, E. Boukris and T. van Harmelen, Sources, Transport, and Accumulation of Different Types of Plastic Litter in Aquatic Environments: A Review Study, *Mar. Pollut. Bull.*, 2019, **143**, 92–100, DOI: 10.1016/j.marpolbul.2019.04.029.

62 K. A. Prather, T. H. Bertram, V. H. Grassian, G. B. Deane, M. D. Stokes, P. J. DeMott, L. I. Aluwihare, B. P. Palenik, F. Azam, J. H. Seinfeld, R. C. Moffet, M. J. Molina, C. D. Cappa, F. M. Geiger, G. C. Roberts, L. M. Russell, A. P. Ault, J. Baltrusaitis, D. B. Collins, C. E. Corrigan, L. A. Cuadra-Rodriguez, C. J. Ebben, S. D. Forestieri, T. L. Guasco, S. P. Hersey, M. J. Kim, W. F. Lambert, R. L. Modini, W. Mui, B. E. Pedler, M. J. Ruppel, O. S. Ryder, N. G. Schoepp, R. C. Sullivan and D. Zhao, Bringing the Ocean into the Laboratory to Probe the Chemical Complexity of Sea Spray Aerosol, *Proc. Natl. Acad. Sci. U.S.A.*, 2013, **110**(19), 7550–7555, DOI: 10.1073/pnas.1300262110.

63 P. J. Wlasits, R. Konrat and P. M. Winkler, Heterogeneous Nucleation of Supersaturated Water Vapor onto Sub-10 nm Nanoplastic Particles, *Environ. Sci. Technol.*, 2023, **57**(4), 1584–1591, DOI: 10.1021/acs.est.2c07643.

64 A. Laaksonen, J. Malila and A. Nenes, Heterogeneous Nucleation of Water Vapor on Different Types of Black Carbon Particles, *Atmos. Chem. Phys.*, 2020, **20**(21), 13579–13589, DOI: 10.5194/acp-20-13579-2020.

65 Y. Wang, H. Okochi, Y. Tani, H. Hayami, Y. Minami, N. Katsumi, M. Takeuchi, A. Sorimachi, Y. Fujii, M. Kajino, K. Adachi, Y. Ishihara, Y. Iwamoto and Y. Niida, Airborne Hydrophilic Microplastics in Cloud Water at High Altitudes and Their Role in Cloud Formation, *Environ. Chem. Lett.*, 2023, DOI: 10.1007/s10311-023-01626-x.

66 A. W. H. Chan, J. H. Kroll, N. L. Ng and J. H. Seinfeld, Kinetic Modeling of Secondary Organic Aerosol Formation: Effects of Particle- and Gas-Phase Reactions of Semivolatile Products, *Atmos. Chem. Phys.*, 2007, **7**(15), 4135–4147, DOI: 10.5194/acp-7-4135-2007.

67 N. M. Donahue, A. L. Robinson, C. O. Stanier and S. N. Pandis, Coupled Partitioning, Dilution, and Chemical Aging of Semivolatile Organics, *Environ. Sci. Technol.*, 2006, **40**(8), 2635–2643, DOI: 10.1021/es052297c.

68 M. Bilde, K. Barsanti, M. Booth, C. D. Cappa, N. M. Donahue, E. U. Emanuelsson, G. McFiggans, U. K. Krieger, C. Marcolli, D. Topping, P. Ziemann, M. Barley, S. Clegg, B. Dennis-Smither, M. Hallquist, Å. M. Hallquist, A. Khlystov, M. Kulmala, D. Mogensen, C. J. Percival, F. Pope, J. P. Reid, M. A. V. Ribeiro da Silva, T. Rosenoern, K. Salo, V. P. Soonsin, T. Yli-Juuti, N. L. Prisle, J. Pagels, J. Rarey, A. A. Zardini and I. Riipinen, Saturation Vapor Pressures and Transition Enthalpies of Low-Volatility Organic Molecules of Atmospheric Relevance: From Dicarboxylic Acids to Complex Mixtures, *Chem. Rev.*, 2015, **115**(10), 4115–4156, DOI: **10.1021/cr5005502**.

69 W.-S. W. DeRieux, Y. Li, P. Lin, J. Laskin, A. Laskin, A. K. Bertram, S. A. Nizkorodov and M. Shiraiwa, Predicting the Glass Transition Temperature and Viscosity of Secondary Organic Material Using Molecular Composition, *Atmos. Chem. Phys.*, 2018, **18**(9), 6331–6351, DOI: **10.5194/acp-18-6331-2018**.

70 A. M. Maclean, N. R. Smith, Y. Li, Y. Huang, A. P. S. Hettiyadura, G. V. Crescenzo, M. Shiraiwa, A. Laskin, S. A. Nizkorodov and A. K. Bertram, Humidity-Dependent Viscosity of Secondary Organic Aerosol from Ozonolysis of β-Caryophyllene: Measurements, Predictions, and Implications, *ACS Earth Space Chem.*, 2021, **5**(2), 305–318, DOI: **10.1021/acsearthspacechem.0c00296**.

71 J. C. Corbin, R. L. Modini and M. Gysel-Beer, Mechanisms of Soot-Aggregate Restructuring and Compaction, *Aerosol Sci. Technol.*, 2023, **57**(2), 89–111, DOI: **10.1080/02786826.2022.2137385**.

72 C. Chen, O. Y. Enekwizu, X. Fan, C. D. Dobrzanski, E. V. Ivanova, Y. Ma, G. Y. Gor and A. F. Khalizov, Single Parameter for Predicting the Morphology of Atmospheric Black Carbon, *Environ. Sci. Technol.*, 2018, **52**(24), 14169–14179, DOI: **10.1021/acs.est.8b04201**.